State of charge estimation of lithium-ion battery using an extended Kalman filter optimized by the octopus optimization algorithm

Kezban Koç Savaş
Department of Electrical and Electronics Engineering,
Grad. Sch. of Natural and Applied Sci.,
Gazi University,
Ankara, Türkiye
kezbankoc@gazi.edu.tr

Mehmet Demirtaş
Department of Electrical and Electronics Engineering,
Faculty of Technology,
Gazi University,
Ankara, Türkiye
mehmetd@gazi.edu.tr

İpek Çetinbaş
Department of Electrical and Electronics Engineering,
Fac. of Engineering and Architecture,
Eskisehir Osmangazi University,
Ankara, Türkiye
ipekcetinbas@ogu.edu.tr

***Abstract*— Reliable state-of-charge (SoC) estimation is a key requirement for the safe and efficient operation of battery management systems (BMSs) in lithium-ion batteries (LiBs). In this study, an extended Kalman filter (EKF)-based SoC estimation approach optimized by the Octopus Optimization Algorithm (OOA) is proposed. The battery dynamics are represented using a first-order RC equivalent circuit model, whose parameters are updated online by the forgetting-factor recursive least squares (FFRLS) method. In addition, the EKF covariance parameters are optimized by OOA to improve estimation performance. The proposed method is evaluated using the dynamic stress test (DST) profile at 25 °C from the University of Maryland battery dataset. For comparison, fixed-ECM EKF, FFRLS-ECM EKF, particle swarm optimization-based EKF (PSO-EKF), and centered collision optimizer-based EKF (CCO-EKF) are implemented under the same conditions. Among the compared methods, OOA-EKF achieves the best SoC estimation performance, with a root mean square error (RMSE) of 0.9727%. Compared with fixed-ECM EKF, OOA-EKF reduces the SoC estimation RMSE by approximately 31.8%. The method also provides accurate terminal voltage tracking, with a voltage RMSE of 0.2996 mV. These findings indicate that combining FFRLS-based time-varying ECM parameters with OOA-optimized EKF covariance parameters improves both SoC estimation accuracy and terminal voltage tracking performance.**

Keywords*— *state of charge, extended Kalman filter, lithium-ion batteries, octopus optimization algorithm, forgetting factor recursive least squares

I. INTRODUCTION

In line with the global energy transition and sustainability goals, LiBs have become one of the key technologies widely used in energy storage systems and electric vehicles owing to their superior characteristics, such as high power capability, high energy density, etc. In this context, LiB technologies play an important role in a wide range of applications [1, 2]. The nonlinear behavior of battery cells and their dependence on operating conditions require an effective BMS to prevent overcharge-overdischarge and improve energy efficiency [3]. Accurate estimation of the current SoC is one of the fundamental functions of a BMS, as it enables the determination of available capacity and the reliable implementation of energy management strategies [4].

SoC is a quantity and cannot be directly measured. Therefore, it must be calculated or estimated indirectly from measurable quantities such as temperature, voltage, and current [5]. SoC estimation methods are commonly categorized into Coulomb counting, open-circuit voltage (OCV)-based methods, data-driven approaches, and model-based closed-loop filtering techniques. Although Coulomb counting is widely used due to its ease of implementation and low computational cost, it is sensitive to uncertainties in the initial SoC value and the accumulation of current measurement errors over time [6]. OCV-based methods can provide reliable results through the OCV–SoC relationship; however, they require long rest periods for the battery to reach equilibrium. This requirement limits their real-time applicability under dynamic driving cycles and varying load conditions [7]. Recently, data-driven SoC estimation has attracted considerable attention, particularly with the use of deep learning and artificial intelligence techniques. These methods are capable of capturing nonlinear relationships between measurable battery signals and SoC; therefore, different network architectures and learning models have been examined in comparative studies [8]. Nevertheless, the performance of these models largely depends on the quality of the training data. Their limited generalization capability under different temperatures, aging levels, and load profiles remains one of the key challenges in applying data-driven methods in practical applications [9]. As an alternative to the limitations encountered in conventional and data-driven methods, model-based estimation approaches, which mathematically represent the electrical behavior of batteries, have been widely used. Among these approaches, the EKF stands out in SoC estimation due to its closed-loop error correction and noise suppression capabilities in nonlinear battery state-space models [10]. However, the accuracy and stability of the EKF are strongly affected by the ECM parameter values, the selected initial conditions, and the tuning of the measurement and process noise covariance matrices [11]. Incorrect determination of these parameters may increase the estimation error and degrade filter performance.

Considering the limited processing capacity of BMS hardware, the Thevenin-type ECM provides a practical solution by representing terminal voltage and polarization effects with low computational burden [12]. During battery operation, the electrical parameters of the ECM are affected by temperature, SoC range, current profile, and aging, which causes them to vary over time [13]. Therefore, models with fixed parameters may not represent battery behavior with sufficient accuracy under dynamic operating conditions and may increase the SoC estimation error. To mitigate this problem, online identification methods and adaptive filtering approaches capable of tracking time-varying parameters have been developed [14].

XXX-X-XXXX-XXXX-X/XX/$XX.00 ©20XX IEEE

Metaheuristic algorithms have recently become a useful tool in battery estimation studies, particularly for identifying ECM parameters and tuning filter-related coefficients [15]. The particle swarm optimization (PSO) has provided effective results in the optimization of nonlinear battery observers, sliding-mode structures, and machine learning-based SoC estimation models [16]. Similarly, the grey wolf optimizer has been used to improve modeling and estimation performance by extracting nonlinear ECM parameters and tuning EKF covariance matrices [17]. These studies demonstrate that optimization-assisted model-based estimation approaches have significant potential for dynamic and nonlinear battery systems.

In this study, an EKF-based SoC estimation approach optimized using the OOA, referred to as OOA-EKF, is proposed to improve estimation performance in LiB under dynamic operating conditions. In the proposed method, the time-varying parameters of the Thevenin or RC equivalent circuit model are updated online using the FFRLS method, while the EKF covariance parameters that directly affect estimation performance are optimized using OOA. In this way, time-dependent variations in the battery model parameters are incorporated into the estimation process, and the filter settings are systematically improved. The main contribution of this study is the integration of OOA into an EKF-based SoC estimation framework with FFRLS-updated ECM parameters and the comparative evaluation of its performance against different EKF-based methods. In this context, the proposed OOA-EKF method is compared with fixed-ECM EKF, FFRLS-ECM EKF, particle swarm optimization-based EKF (PSO-EKF), and centered collision optimizer-based EKF (CCO-EKF) under the same operating conditions. All methods are evaluated in terms of SoC estimation accuracy, terminal voltage tracking performance, and error metrics.

II. MATERIALS AND METHODS

This section details the structure of the proposed OOA-EKF-based SoC estimation framework. First, the first-order RC model employed to represent the dynamic response of the LiB is presented. The FFRLS-based online identification procedure is then introduced to update the time-varying model parameters, followed by the EKF formulation used for SoC estimation. Finally, the EKF covariance tuning problem is defined for the optimization-based selection of the filter parameters.

A. First-order RC model

In this study, the electrical behavior of the LiB is modeled using the first-order RC equivalent circuit shown in Fig. 1. The model includes an OCV source, an ohmic resistance (R_0), and a parallel ($R_P - C_P$) network that represents the polarization dynamics of the cell. Since this structure can capture the main terminal voltage response with relatively low computational complexity, it is suitable for SoC estimation applications. Assuming that the discharge current is positive, the discrete-time dynamics of the polarization voltage are first described in (1). Using the updated polarization voltage, the terminal voltage of the cell is then expressed in (2). The coefficients $a(k)$ and $b(k)$, which determine the dynamic response of the polarization branch, are defined in (3) and (4), respectively. Finally, the time update of SoC is performed based on Coulomb counting, as given in (5).

$$V_P(k) = b(k-1)I_L(k-1) + a(k-1)V_P(k-1) \quad (1)$$

$$V_{term}(k) = OCV\big(SoC(k)\big) - V_P(k) - I_L(k)R_0(k) \quad (2)$$

$$a(k) = \exp\left(-\frac{\Delta t}{R_P(k)C_P(k)}\right) \quad (3)$$

$$b(k) = R_P(k)\left[1 - exp\left(-\frac{\Delta t}{R_P(k)C_P(k)}\right)\right] \quad (4)$$

$$SoC(k) = SoC(k-1) - \frac{\eta \Delta t}{3600 Q_n} I_L(k-1) \quad (5)$$

In these equations, $R_0(k)$ represents the ohmic resistance, while $C_P(k)$ and $R_P(k)$ correspond to the polarization capacitance and resistance of the RC branch, respectively. V_{term} denotes the measured terminal voltage, $V_P(k)$ is the polarization voltage, and $I_L(k)$ is the load current. The term $OCV(SoC(k))$ describes the OCV–SoC relationship used in the model. Furthermore, Δt, Q_n and η indicate the sampling time, nominal capacity, and Columbic efficiency, respectively. Because the ECM parameters are affected by operating conditions, they are updated online through the FFRLS method.

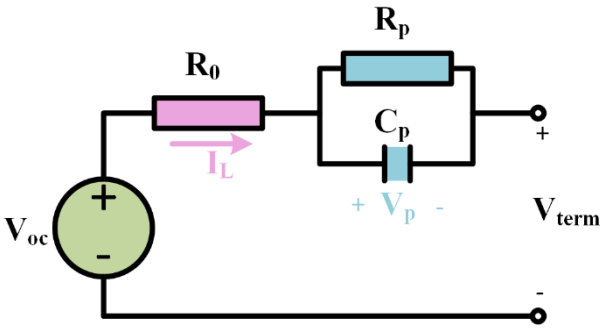

Fig. 1. First-order RC model

B. FFRLS-based parameter estimation

The parameters of the first-order RC model may vary depending on operating conditions such as temperature, current profile, SoC range, and aging. Therefore, in this study, the FFRLS method is used to update the ECM parameters online. In the FFRLS algorithm, the difference between the model output $y(k)$ and the estimated output $\hat{y}(k)$ is defined as the error term in (6). The covariance matrix ($P(k)$), gain vector ($K(k)$), and parameter vector ($\hat{\theta}(k)$) are then updated using (7)–(9), respectively.

$$e(k) = y(k) - \hat{y}(k) \quad (6)$$

$$P(k) = \frac{1}{\lambda}[P(k-1) - K(k)\phi(k)^T P(k-1)] \quad (7)$$

$$K(k) = \frac{P(k-1)\phi(k)}{\lambda + \phi(k)^T P(k-1)\phi(k)} \quad (8)$$

$$\hat{\theta}(k) = \hat{\theta}(k-1) + K(k)e(k) \quad (9)$$

Where, $\phi(k)$ is the regression vector, $\hat{\theta}(k)$ is the estimated parameter vector, and λ is the forgetting factor. The parameters are calculated from the discrete-time model coefficients obtained by FFRLS using (10)–(12). Thus, the time-varying parameters $\hat{R}_0$, $\hat{R}_P$, and $\hat{C}_P$ obtained by the

FFRLS method are used as the updated battery model in the EKF-based SoC estimation process.

$$\hat{R}_0 = \hat{\theta}_2 \tag{10}$$

$$\hat{R}_P = \frac{\hat{b}}{1-\hat{a}} \tag{11}$$

$$\hat{C}_P = -\frac{\Delta t}{\hat{R}_1 \ln(\hat{a})} \tag{12}$$

C. EKF-based SoC estimation

In this study, SoC estimation is performed using the EKF method with the time-varying ECM parameters updated by FFRLS. In the EKF structure, the state vector is defined in (13) by considering the battery SoC and the polarization voltage. Using the battery current and the FFRLS-updated ECM parameters, the predicted state vector is obtained in (14). The predicted error covariance matrix is calculated using (15), and the Jacobian matrix is defined in (16). The terminal voltage measurement function is expressed in (17), while its measurement Jacobian matrix (F_k) is given in (18). In the measurement update stage, the Kalman gain (K_k) is calculated using (19). Finally, the state vector and the error covariance matrix are updated using (20) and (21), respectively.

$$x_k = [SoC_k \quad V_{P,k}]^T \tag{13}$$

$$\hat{x}_{k|k-1} = \begin{bmatrix} \widehat{SoC}_{k-1|k-1} - I_{L|k-1}(\eta \Delta t)/3600Q_n \\ a_{k-1}\hat{V}_{P,k-1|k-1} + I_{L|k-1}b_{k-1} \end{bmatrix} \tag{14}$$

$$P_{k|k-1} = F_k P_{k-1|k-1} F_k^T + Q \tag{15}$$

$$F_k = [1\ 0; 0\ a_{k-1}] \tag{16}$$

$$\hat{V}_{term,k} = OCV\left(\widehat{SoC}_{k-1|k-1}\right) - R_{0,k} I_{L|k} - \hat{V}_{P,k|k-1} \tag{17}$$

$$H_k = [\frac{dVocv}{dSoC} - 1] \tag{18}$$

$$K_k = P_{k|k-1} H_k^T (H_k P_{k|k-1} H_k^T + R)^{-1} \tag{19}$$

$$\hat{x}_{k|k} = \hat{x}_{k|k-1} + K_k(V_{term,k} - \hat{V}_{term,k}) \tag{20}$$

$$P_{k|k} = (IK_k H_k) P_{k|k-1} \tag{21}$$

Here, x_k denotes the state vector, and SoC_k represents the state of charge of the battery. $\hat{x}_{k|k-1}$ denotes the predicted state vector before the measurement update, while $\hat{x}_{k|k}$ represents the updated state vector after the measurement update. Similarly, $P_{k|k-1}$ is the predicted error covariance matrix, and $P_{k|k}$ is the updated error covariance matrix. In addition, F_k denotes the state-transition Jacobian matrix, Q is the process noise covariance matrix, and R is the measurement noise covariance. The term $\frac{dVocv}{dSoC}$ in (18) is obtained from the OCV–SoC curve used in this study. Since the estimation performance of the EKF is sensitive to the appropriate selection of the Q and R covariance parameters, these filter parameters are determined using metaheuristic optimization algorithms in this study.

D. Optimization problem formulation for EKF covariance parameters

In EKF-based SoC estimation, the Q and R have a significant effect on the convergence speed, stability, and estimation accuracy of the filter. Selecting inappropriate values for these parameters may increase the SoC estimation error or make the filter overly sensitive to measurement noise. Therefore, in this study, the covariance parameters of the EKF are treated as an optimization problem. Since the EKF state vector consists of two state variables, namely SoC and V_P, the process noise covariance matrix is defined in diagonal form. The measurement noise covariance associated with the terminal voltage measurement is used as a scalar parameter. The decision variable updated by the optimization algorithms is given in (22). These variables are defined on a logarithmic scale. The logarithmic search space enables small-magnitude covariance values to be explored in a more balanced and effective manner.

$$X = \left[q_{SoC}, q_{V_P}, r_V\right] \tag{22}$$

In the optimization process, the objective function is defined to jointly consider SoC estimation accuracy, and terminal voltage tracking performance. In this context, the objective function to be minimized is given in (23).

$$J(X) = w_{SoC} \times RMSE_{SoC} + w_{Vterm} \times RMSE_{Vterm} \tag{23}$$

Where, $RMSE_{SoC}$ indicates the estimation error between the reference SoC and the EKF-estimated SoC, while $RMSE_{Vterm}$ represents the error between the measured and estimated terminal voltages. The coefficients w_{SoC} and w_{Vterm} define the relative weights assigned to the SoC estimation error and terminal voltage tracking error. The aim of the optimization algorithm is to determine the EKF covariance parameters that minimize the objective function $J(X)$ given in (23).

E. Octopus optimization algorithm

The OOA algorithm was proposed by Wang et al. in 2026. OOA is inspired by the natural behaviors of marine octopuses, including prey searching, prey capture, escaping from potential threats, and mating strategies. These biological processes, ranging from hunting to mating, are mathematically modeled in OOA to guide individuals in the population toward the optimal solution within the search space of the defined problem. The algorithmic structure is organized into two main search phases. These two phases are referred to as exploration and exploitation. In the exploration phase, the prey-searching, attacking, capturing, and threat-avoidance behaviors of octopuses are simulated. In this phase, the recoil motion generated by water jet propulsion corresponds to the ability of individuals in the

$$Exploration = \begin{cases} Search & \begin{cases} X_i^{t+1} = X_i^t + V_i^{t+1} \\ V_i^{t+1} = FV_i^t + A_1 e^{-\beta_2\sqrt{r_0}(t/T_{OOA})}\left(X_{k_0}^t - X_i^t\right) + A_3 e^{-\beta_1\sqrt{r_{i_{best}}}\left(1-\sqrt{t/T_{OOA}}\right)}\left(X_{i_{best}}^t - X_i^t\right) \end{cases} \\ Escape & \begin{cases} X_i^{t+1} = X_i^t + V_i^{t+1} + |A|(((V_i^t)^2 - (V_i^{t-1})^2)/(2\cdot al)), \quad |A| > 1 \\ V_i^{t+1} = FV_i^t + A_1 e^{-\beta_2\sqrt{r_1}(t/T_{OOA})}\left(X_{k_1}^t - X_i^t\right) + A_1 e^{-\beta_2\sqrt{r_2}(t/T_{OOA})}\left(X_{k_2}^t - X_i^t\right) \end{cases} \\ Attack & \begin{cases} X_i^{t+1} = X_i^t + V_i^{t+1} + |A|(((V_i^t)^2 - (V_i^{t-1})^2)/(2\cdot al)), \quad |A| \le 1 \\ V_i^{t+1} = FV_i^t + A_3 e^{-\beta_1\sqrt{r_{i_{best}}}\left(1-\sqrt{t/T_{OOA}}\right)}\left(X_{i_{best}}^t - X_i^t\right) + A_2 e^{-\beta_3\sqrt{r_{gbest}}(1-t/T_{OOA})}\left(X_{gbest}^t - X_i^t\right) \end{cases} \end{cases} \quad (24)$$

$$Exploitation = \begin{cases} Close-range & \left\{X_i^{t+1} = pK_{1X}^t + (1-p)K_{2X}^t \quad if \quad 0 < R \le pl\right. \\ Medium-range & \left\{X_i^{t+1} = rand\cdot K_{2X}^t \quad if \quad R > pl\right. \\ Deep\ local & \left\{X_i^{t+1} = rand\cdot K_{2X}^t + K_{1X}^t \quad if \quad R = 0\right. \end{cases} \quad (25)$$

population to explore different regions of the search space and avoid local optima. In the exploitation phase, different mating strategies of octopuses are imitated. This mechanism enables a more detailed search of promising regions and supports local intensification around high-quality solutions. The mathematical framework of OOA, which balances the exploration and exploitation phases, is given in (24) and (25).

In these equations, X_i^t and X_i^{t+1} denote the current and updated positions of the ith octopus, respectively. V_i^{t-1}, V_i^t, and V_i^{t+1} represent the previous, current, and updated inertial velocities. F is the fluid resistance coefficient, t is the current iteration, and T_{OOA} is the maximum number of iterations. A_1, A_2, and A_3 are the attraction strength coefficients, while β_1, β_2, and β_3 are the perception coefficients. $X_{k_0}^t$, $X_{k_1}^t$, and $X_{k_2}^t$ denote randomly selected positions. $X_{i_{best}}^t$ and X_{gbest}^t represent the individual best position and the global best position, respectively. In addition, r_0, r_1, r_2, $r_{i_{best}}$, and r_{gbest} denote the distances between the current position and the corresponding reference positions. $|A|$ is the acceleration intensity parameter, a is a time-varying parameter, and al is the recoil acceleration parameter. K_{1X}^t and K_{2X}^t represent the male and female octopus positions, respectively. p is the mating coefficient, R is the distance between female and male octopuses, $rand$ is a random number, and pl is the safe mating distance threshold [18].

To evaluate the comparative performance of the proposed OOA-EKF, the same optimization problem was also solved using the PSO and CCO algorithms. In all algorithms, the decision vector given in (22) was used as the decision variable, and the same objective function defined in (23) was minimized. To ensure a fair comparison, all algorithms were executed using the same conditions such as population size, maximum number of iterations, and lower and upper boundary values. The control parameters of the optimization algorithms used in this study are given in Table 1.

III. Simulation Results and Discussion

In this section, the SoC estimation performance of the proposed OOA-EKF approach is evaluated using experimental battery data. In the simulation studies, the publicly available LiB dataset provided by the CALCE was used. In this context, the DST profile obtained at 25 °C was considered. All methods were tested under the same comditions and were simulated in MATLAB R2023b.

For the optimization of the EKF covariance parameters, the lower and upper bounds of the decision variables were defined on a logarithmic scale as ([-12, -8, -6]) and ([-5, -3, -2]), respectively. In the comparative analysis, fixed-ECM EKF, FFRLS-ECM EKF, PSO-EKF, CCO-EKF, and the proposed OOA-EKF methods were evaluated In the fixed-ECM EKF approach, the constant values of (R_0, R_P and C_P were determined by taking the average values of the time-varying parameters obtained using FFRLS. In the manually tuned EKF methods, the EKF tuning parameters were selected as $q_{SoC} = 10^{-6}$, $q_{V_P} = 10^{-5}$, and $r_V = 10^{-4}$, respectively. In the optimization-based methods, the Q and R covariance parameters were determined using the PSO, CCO, and OOA algorithms. Thus, the effects of both FFRLS-based time-varying model parameters and optimization-based EKF covariance selection on SoC estimation performance were comparatively investigated.

TABLE I. Main Control Parameters and Settings of the Optimization Algorithms

Algorithm	Inspiration	Control Parameter	Values
OOA [18]	Marine octopus hunting and mating behaviors	Safe mating distance threshold Perception coefficient for potential prey Perception coefficient for natural predators Perception coefficient for prey Population size Maximum number of iterations	w=1.5 pl=12 β_1=0.5 β_2=0.25 β_3=0.75 N_{OOA}=30 T_{OAA}=50
CCO [19]	Head-on collision equations in classical physics	Population size Maximum number of iterations	N_{CCO}=30 T_{CCO}=50
PSO [20]	Swarm behavior	Inertia weight Cognitive and social coefficient Population size Maximum number of iterations	$w = 0.9$ $c_1 = 1.5$, $c_1 = 2$ N_{PSO}=30 T_{PSO}=50

The comparative results for SoC estimation accuracy and terminal voltage tracking are reported in Table 2. In the fixed-ECM EKF method, $RMSE_{SoC}$ and MAE_{SoC} were obtained as 1.4259% and 1.1487%, respectively. When the time-varying ECM parameters updated by FFRLS were used in the FFRLS-ECM EKF method, these values decreased to 1.3472% and 1.0678%, respectively. This result indicates that updating the ECM parameters in a time-varying manner, instead of assuming them to be constant, improves SoC estimation accuracy. When the optimization-based methods are examined, PSO-EKF and CCO-EKF produced very similar SoC estimation results. The $RMSE_{SoC}$ values of these methods were calculated as

1.2300% and 1.2293%, respectively. The proposed OOA-EKF method achieved the lowest SoC estimation error, with $RMSE_{SoC}$ and MAE_{SoC} values of 0.9727% and 0.5082%, respectively. Compared with fixed-ECM EKF, FFRLS-ECM EKF, and PSO-EKF, the proposed OOA-EKF method reduced $RMSE_{SoC}$ by approximately 31.8%, 27.8%, and 20.9%, respectively. Similarly, in terms of MAE_{SoC}, the proposed method provided an improvement of approximately 55.8% compared with fixed-ECM EKF. The SoC estimation curves shown in Fig. 2 also support these numerical results. Although all methods were able to track the reference SoC variation, more pronounced deviations were observed in the fixed-ECM EKF approach. The enlarged view further shows that the proposed OOA-EKF method follows the reference SoC curve more closely and provides a more stable tracking performance, particularly in regions where small deviations occur.

TABLE II. PERFORMANCE COMPARISON OF SOC ESTIMATION AND VOLTAGE TRACKING

Method	$RMSE_{SoC}$ (%)	MAE_{SoC} (%)	$RMSE_{Vterm}$ (mV)	MAE_{Vterm} (mV)
Fixed-ECM EKF	1.4259	1.1487	1.5152	0.7236
FFRLS-ECM EKF	1.3472	1.0678	1.1841	0.7857
PSO-EKF	1.2300	0.8526	0.3005	0.0102
CCO-EKF	1.2293	0.8525	1.0015	0.5342
OOA-EKF	0.9727	0.5082	0.2996	0.0063

The results given in Table 2 also support the effectiveness of the proposed method in terms of terminal voltage tracking performance. While the $RMSE_{Vterm}$ value was 1.5152 mV for the fixed-ECM EKF method, it decreased to 1.1841 mV for the FFRLS-ECM EKF method. Among the optimization-based methods, OOA-EKF achieved one of the most successful results, with $RMSE_{Vterm}$ and MAE_{Vterm} values of 0.2996 mV and 0.0063 mV, respectively. Although PSO-EKF produced a voltage RMSE value very close to that of OOA-EKF, OOA-EKF provided a lower error in terms of MAE_{Vterm}. CCO-EKF, on the other hand, produced SoC estimation results close to those of PSO-EKF, but yielded higher errors n terminal voltage tracking performance. The terminal voltage tracking curves shown in Fig. 3 indicate that the optimization-based methods track the measured terminal voltage more successfully than the manually tuned EKF approaches. In the enlarged view, it is clearly observed that OOA-EKF exhibits a tracking behavior very close to the measured terminal voltage. These results show that the EKF covariance parameters optimized by OOA improve not only SoC estimation accuracy but also terminal voltage tracking performance.

IV. CONLUSION

In this study, an OOA-optimized EKF-based approach was proposed for SoC estimation in LiBs. The simulation results showed that the use of FFRLS-updated time-varying ECM parameters improved SoC estimation performance compared with the fixed-ECM EKF approach. In addition, optimization-based EKF structures further reduced the estimation error by systematically determining the filter covariance parameters. Among the compared methods, the proposed OOA-EKF method achieved the best performance in SoC estimation, with a RMSE of 0.9727% and a mean absolute error of 0.5082%. The proposed method reduced the SoC estimation error by approximately 31.8% compared with fixed-ECM EKF, 27.8% compared with FFRLS-ECM EKF, and 20.9% compared with PSO-EKF. The terminal voltage tracking results also supported the effectiveness of the proposed approach. OOA-EKF produced low voltage tracking errors, with a RMSE of 0.2996 mV and a mean absolute error of 0.0063 mV for the terminal voltage. These results demonstrate that the EKF covariance parameters optimized by OOA improve not only SoC estimation accuracy but also terminal voltage tracking performance. Overall, the proposed OOA-EKF approach can be considered an effective method for LiB SoC estimation under dynamic operating conditions. In future studies, the proposed method will be tested under different temperatures and dynamic driving profiles to evaluate its generalization and robustness performance more comprehensively.

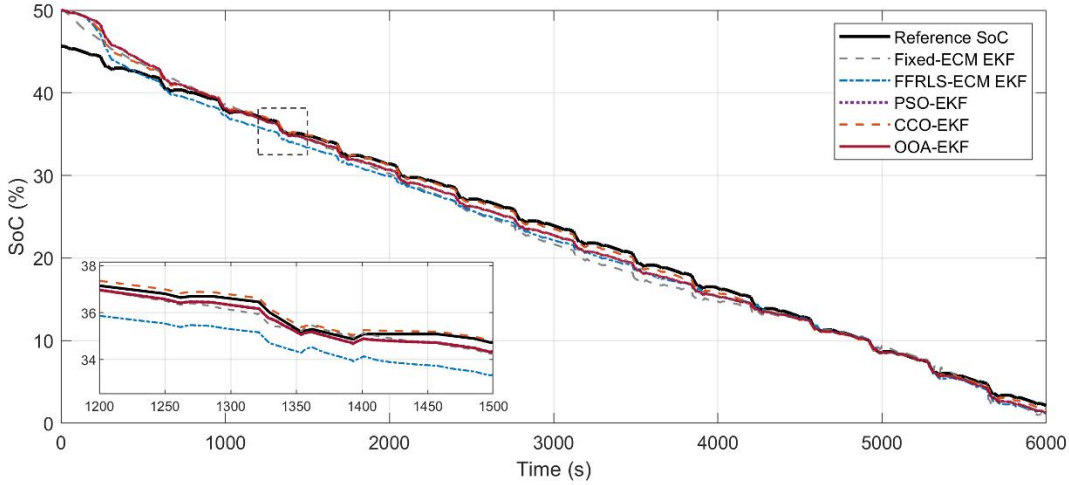

Fig. 2. Comparison of SoC estimation results under the DST test at 25 °C

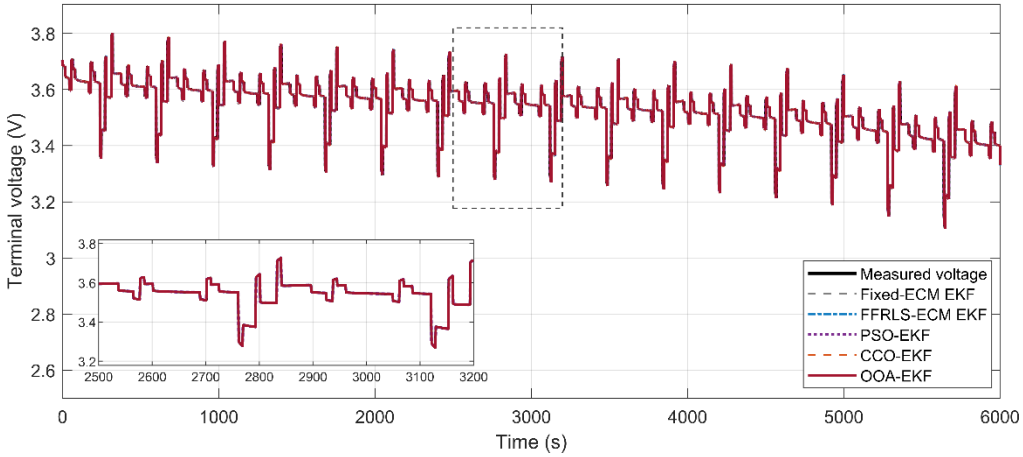

Fig. 3. Comparison of terminal voltage tracking results under the DST test at 25 °C

REFERENCES

[1] H. Xu, Q. Xu, F. Duanmu, J. Shen, L. Jin, B. Gou, *et al.*, "State-of-charge estimation of lithium-ion batteries based on EKF integrated with PSO-LSTM for electric vehicles," *IEEE Transactions on Transportation Electrification,* vol. 11, pp. 2311-2321, 2024.

[2] Y. Miao, P. Hynan, A. Von Jouanne, and A. Yokochi, "Current Li-ion battery technologies in electric vehicles and opportunities for advancements," *Energies,* vol. 12, p. 1074, 2019.

[3] X. Lu, M. Chen, and Y. Tian, "Accurate state-of-charge estimation of LiFePO4 battery: An adaptive extended kalman filter approach using particle swarm optimization," *Energy Reports,* vol. 14, pp. 1169-1178, 2025.

[4] M. A. Hannan, D. N. How, M. H. Lipu, M. Mansor, P. J. Ker, Z. Dong, *et al.*, "Deep learning approach towards accurate state of charge estimation for lithium-ion batteries using self-supervised transformer model," *Scientific reports,* vol. 11, p. 19541, 2021.

[5] C. Vidal, P. Malysz, P. Kollmeyer, and A. Emadi, "Machine learning applied to electrified vehicle battery state of charge and state of health estimation: State-of-the-art," *Ieee Access,* vol. 8, pp. 52796-52814, 2020.

[6] B. Liu, H. Wang, M.-L. Tseng, and Z. Li, "State of charge estimation for lithium-ion batteries based on improved barnacle mating optimizer and support vector machine," *Journal of Energy Storage,* vol. 55, p. 105830, 2022.

[7] Y. Xing, W. He, M. Pecht, and K. L. Tsui, "State of charge estimation of lithium-ion batteries using the open-circuit voltage at various ambient temperatures," *Applied energy,* vol. 113, pp. 106-115, 2014.

[8] N. E. H. Korbaa, N. Bouchetata, A. W. Belarbi, K. Kayisli, and O. Kaplan, "Comparative Study of Different Deep Learning Approaches for State of Charge Estimation in Lithium Iron Phosphate Battery," in *2024 12th International Conference on Smart Grid (icSmartGrid)*, 2024, pp. 714-718.

[9] M. H. Lipu, M. A. Hannan, A. Hussain, M. Hoque, P. J. Ker, M. H. M. Saad, *et al.*, "A review of state of health and remaining useful life estimation methods for lithium-ion battery in electric vehicles: Challenges and recommendations," *Journal of cleaner production,* vol. 205, pp. 115-133, 2018.

[10] S. Wang, K. Ou, W. Zhang, and Y.-X. Wang, "A state-of-charge and state-of-health joint estimation method of lithium-ion battery based on temperature-dependent extended Kalman filter and deep learning," *IEEE Transactions on Industrial Electronics,* vol. 72, pp. 570-579, 2024.

[11] T. Chaudhari, "State of charge estimation of sustainable low emission electrochemical energy storage systems," *Turkish Journal of Engineering,* vol. 10, pp. 689-706, 2026.

[12] K. K. Savas, M. Demirtaş, and İ. Çetinbaş, "Comprehensive parameter estimation for lithium-ion battery model using escape algorithm," *Journal of Energy Storage,* vol. 131, p. 117476, 2025.

[13] H. Wang, Y. Zheng, and Y. Yu, "Lithium-ion battery SOC estimation based on adaptive forgetting factor least squares online identification and unscented Kalman filter," *Mathematics,* vol. 9, p. 1733, 2021.

[14] W. Song, R. Liu, X. Jin, and W. Guo, "SOC Estimation for Lithium-Ion Batteries Based on Weighted Multi-Innovation Sage–Husa Adaptive EKF," *Energies,* vol. 18, p. 4364, 2025.

[15] K. K. Savaş, M. Demirtaş, and İ. Çetinbaş, "Parameter Estimation with Phototropic Growth Algorithm and Cape Lynx Optimizer for Lithium-Ion Battery," in *2025 14th International Conference on Renewable Energy Research and Applications (ICRERA)*, 2025, pp. 979-984.

[16] C. Zhang, S. Wang, C. Yu, Y. Xie, and C. Fernandez, "Novel improved particle swarm optimization-extreme learning machine algorithm for state of charge estimation of lithium-ion batteries," *Industrial & Engineering Chemistry Research,* vol. 61, pp. 17209-17217, 2022.

[17] O. Oubraik, H. Oufettoul, M. Aannir, and I. Saadoune, "Non-Linear Equivalent Circuit Model Parameters Extraction Using Grey Wolf Optimizer for Enhanced Battery Modeling," in *2025 13th International Conference on Smart Grid (icSmartGrid)*, 2025, pp. 67-74.

[18] K. Wang, L. Abualigah, A. Smerat, J. Li, X. Wu, H. Liu, *et al.*, "A nature recoil mechanism-based Octopus Optimization Algorithm for solving the global and constraint optimization from engineering structural design problems," *Journal of Computational Design and Engineering,* vol. 13, pp. 123-232, 2026.

[19] Y. Lang, Y. Gao, T. Chen, and H. Wang, "Centered Collision Optimizer: A novel and efficient physics-based metaheuristic optimization algorithm for solving complex real-world engineering optimization problems," *Computer Methods in Applied Mechanics and Engineering,* vol. 448, p. 118491, 2026.

[20] J. Kennedy and R. Eberhart, "Particle swarm optimization," in *Proceedings of ICNN'95-international conference on neural networks*, 1995, pp. 1942-1948.